Research Square

Preprints are preliminary reports that have not undergone peer review.
They should not be considered conclusive, used to inform clinical practice,
or referenced by the media as validated information.

In Silico Polypharmacological Profiling of Lupeol and 1-Heptatriacontanol from Probiotic Limosilactobacillus reuteri GM4 and Streptococcus equinus WC1 against Colorectal Cancer-Associated Targets

Mona A. Ashour
Ain Shams University, Faculty of Agriculture
Khaled Metwally
khaleda.fatah@agr.asu.edu.eg

Ain Shams University, Faculty of Agriculture

Research Article

Keywords: Gut microbiota, Lupeol, 1-Heptatriacontanol, Colorectal cancer, GC-MS, Molecular docking

Posted Date: November 13th, 2026

DOI: https://doi.org/10.21203/rs.3.rs-10913054/v1

License: This work is licensed under a Creative Commons Attribution 4.0 International License.
Read Full License

Additional Declarations: No competing interests reported.

In Silico Polypharmacological Profiling of Lupeol and 1-Heptatriacontanol from Probiotic *Limosilactobacillus reuteri* GM4 and *Streptococcus equinus* WC1 against Colorectal Cancer-Associated Targets

Mona A. Ashour[1] & Khaled Metwally[2*]

1 Department of Agricultural Microbiology, Faculty of Agriculture, Ain Shams University, Cairo 11241, Egypt; Mona.ashor@agr.asu.edu.eg, Orcid ID: 0000-0002-0297-7945

2 Department of Genetics, Faculty of Agriculture, Ain Shams University, Cairo, Egypt; khaleda.fatah@agr.asu.edu.eg, Orcid ID: 0000-0002-9560-9171

*Corresponding author: **khaleda.fatah@agr.asu.edu.eg**

Abstract

Cancer's molecular wiring is notoriously hard to untangle, so computational tools have become essential for mapping disease mechanisms and narrowing down therapeutic leads. Here, we applied *in silico* screening to evaluate the anticancer potential of metabolites from two probiotic gut isolates: *Streptococcus equinus* WC1 (SE-WC1) and *Limosilactobacillus reuteri* GM4 (LR-GM4). Lactic acid bacteria are core members of the human gut microbiota, and their metabolic repertoire—ranging from pathogen suppression to immune modulation and vitamin synthesis—has attracted growing scientific attention. GC–MS profiling of volatile hydrocarbons identified lupeol (14.49%) and 1-heptatriacontanol (5.48%) as the major bioactive constituents, with lupeol detectable in both strains at differing abundances.

Docking simulations against ten cancer-linked proteins revealed that lupeol bound more strongly than 1-heptatriacontanol at eight out of ten targets. Its calculated free energies ran from −6.2 kcal/mol (NR1I3) down to −11.0 kcal/mol (HSD11B1), whereas 1-heptatriacontanol managed only −3.2 kcal/mol (SHH) to −6.8 kcal/mol (UGT2B7). The energy gap (ΔΔG) was smallest at GPBAR1 (−0.4 kcal/mol) and largest at HSD11B1 (−4.7 kcal/mol), with intermediate differences at AR (−4.0), SHH (−3.9), CDC25B (−3.4), and TRPM8 (−3.0 kcal/mol). Because lupeol successfully engaged structurally unrelated proteins—nuclear receptors, phosphatases, ion channels, and metabolic enzymes alike—its superior binding appears to stem from inherent scaffold properties rather than target-specific recognition.

Keywords:

Gut microbiota, Lupeol, 1-Heptatriacontanol, Colorectal cancer, GC-MS, Molecular docking

Introduction

The death rate and morbid are primarily caused by the development and progression of cancerous tumors, as well as the inflammation that is associated with the tumors, all over the world [1]. The most prevalent cancer of the gastrointestinal (GI) tract is now colorectal cancer (CRC) [2]. It is the second leading cause of cancer-related deaths globally, with an annual diagnosis rate of roughly 10% [3, 4]. The World Health Organization (WHO) projects that by 2030, there will be roughly

75 million cases of colorectal cancer (CRC), a markedly higher death rate [5]. According to [6], colorectal cancer (CRC) is the third most common malignancy in men after prostate cancer and the second most common disease in women after breast cancer. The incidence and prevalence of colorectal cancer are generally rising due to the aging of the population and the growth in established risk factors such obesity, sedentary lifestyles, smoking, and chronic inflammatory disorders [7, 8].

Multiple cancer treatments are costly and time-consuming, including surgery, chemotherapy, radiation therapy, immunotherapy, hormone therapy, and combinations of these treatments. A cancer treatment's efficacy is determined by how well it kills cancer cells with the least amount of adverse effects on healthy cells [9]. Terpenoids, and Alkaloids are only two examples of the many bioactive compounds that bacteria can make. These compounds have a range of biological and medicinal uses, some of which may be helpful in maintaining the health of people and animals [10]. Probiotics are live, non-pathogenic microorganisms [11]. Probiotics, which are active microorganisms that benefit the host, can either directly prevent excessive apoptosis or induce it in abnormal cells while protecting normal cells. They can do this by secreting metabolites or by controlling host signaling pathways like Bcl-2/Bax, caspase cascades, and important anticancer pathways. As demonstrated by *Lactobacillus plantarum*, *Lactobacillus Reuteri, Lactobacillus rhamnosus*, and others, these pathways help to alleviate pathological disorders [12–15].

Probiotics observed in liver and colon cancer have been found to induce apoptosis through core apoptotic pathways similar to antitumor drugs, involving AKT, RAS, Raf, MEK, ERK, and mTOR kinase signaling pathways [16–20], and inhibiting growth factor receptors such as EGFR, Her2/Neu, other ERBB family members, c-Met, and NTRK [21–26].

Due to sedentary lifestyles and poor dietary choices, colon cancer has become the second most common cause of cancer-related death globally in recent years [27]. According to recent research, probiotic supplements may be superior to conventional medications in some cancer therapies and their adverse effects. Probiotics can improve intestinal barrier function, gut microbiota, immunological response, and minimize harmful side effects when taken as adjuvant therapy [28]. One of the main objectives of developing cancer treatments is to induce apoptosis in cancer cells [29]. Interestingly, the consumption of beneficial bacteria or probiotics with food supplements can reconstitute the disrupted equilibrium of the gut microbiota [30]. Probiotic formulations may also be helpful in reducing the incidence of colorectal cancer (CRC) and postoperative problems in CRC patients, according to clinical research [31, 32]. The precise mechanism is unclear, despite reports that probiotics reduce chronic inflammatory and carcinogenic activities in the colon that cause colorectal cancer (CRC) and reduce treatment toxicity recurrence.

In the advancement of computer-aided design and molecular biology, molecular docking is a helpful tool. Predicting biological activity is the aim of ligand-protein binding. In order to uncover new knowledge from intricate biological relationships, computational models and network-based approaches can create association networks using data from databases and published literature. This makes it possible to identify the key target molecules participating in these interactions, see the global picture of the pertinent biological interactions, and locate the

hidden link. Additionally, ligand-target interactions at the molecular level can be estimated with the help of molecular docking studies [33]. Thus, the purpose of this work was to use molecular docking analysis to investigate the bioactive secondary metabolite effects of two probiotic strains: *Streptococcus equinus* WC1 PP900644 (SE-WC1) and *Limosilactobacillus reuteri* GM4 PP900643 (LR-GM4) on human colon cancer.

Materials and Method

1. Microorganisms

The bacterial strains, *Streptococcus equinus* WC1 PP900644 (SE-WC1) and *Limosilactobacillus reuteri* GM4 PP900643 (LR-GM4) stains was collected from Agricultural Microbiology Department, Faculty of Agriculture, Ain Shams University, Cairo, Egypt.

2. Bioactive compounds

2.1. Extraction of Bioactive Metabolites

Erlenmeyer flasks containing MRS medium were inoculated with a 48 h the probiotic strains *Limosilactobacillus reuteri* GM_4 and *Streptococcus equinus* WC_1 and the flasks were kept at 37 °C for 48 h. The bacterial supernatant was separated by centrifugation (1500 × g, 10 min, 4 °C). The resulting supernatant was extracted using ethyl acetate according to [34].

2.2.GC–MS Analysis

A coupled Varian GC–MS (Perkin Elmer Auto XL GC, Waltham, MA, USA) equipped with a flame ionization detector was used for the analysis as described previously [35]. The quantification of the identified components was investigated using a percent relative peak area. Tentative identification of the compounds was performed based on relative retention time comparison and mass spectra with those of the NIST, WILLY, Mainlib and Replib library data of the GC/MS system [35, 36].

3. Molecular docking study.

3.1. Ligand Preparation

The ligands used in this study, 1-Heptatriacotanol (PubChem CID 537071), and Lupeol (PubChem CID 259846), were retrieved from PubChem. Energy minimization was performed using the MMFF94 force field [37] implemented in Avogadro 1.2.0 [38] to obtain optimized conformations.

3.2 Protein preparation

Target proteins were selected based on screening of the ligands using SwissTargetPrediction [39]. The structures of the following human targets—AR (P10275),

CDC25A (P30304), CDC25B (P30305), GPBAR1 (Q8TDU6), HSD11B1 (P28845) NR1I3 (Q14994), POLB (P06746), SHH (Q15465), TRPM8 (Q7Z2W7), and UGT2B7 (P16662)—were retrieved from the UniProt database in the format of Alphafold (.PDB). The binding sites were predicted based on literature data and validated using the CB-Dock2 server [40]. Proteins were prepared for docking using AutoDock Tools 1.5.7 [41], which involved adding polar hydrogens, and assigning Gasteiger charges.

3.3Active Site Prediction and Molecular Docking

The binding sites for each protein were predicted using the CB-Dock2 server (4), which implements a cavity detection algorithm to identify potential binding pockets. Molecular docking simulations were performed using QuickVina 2 (QVina2) [42] to evaluate ligand–protein binding interactions. Visualization of the predicted interaction complexes were predicted using Biovia Discovery studio visualizer software v25.1(Dassault Systèmes BIOVIA, San Diego, CA, USA).

Results

1. GC–MS Analysis of Metabolic Products of the Bacterial Strains

Lupeol (14.49%), α-Sitos-terol (5.23%), stigmast-5-en-3-ol (3á)- (5.23%), Ç-sitos-terol (5.23%), stigmast-5-en-3-ol (3á,24S)- (5.23%), and lup-20(29)-En-3-Yl acetate (3.53%) According to GC–MS results of the volatile hydrocarbon of SE-WC_1 strain (**Table 1& Fig. 1**) showed the identification of the major bioactive compounds based on the area percentage. However, bioactive chemicals were found in the volatile components of the LR-GM4extract according to the GC–MS results (**Table 2 & Fig. 2**). The major compounds based on the area percentage were 1-Heptatriacotanol (5.48%), methyl commate D (5.48%), 9,19-cyclolanost-24-en-3-ol, acetate (3á)- (4.09%), lupeol (4.09%), lup-20(29)-en-28-al, 3-(trimethylsilyl)oxy (3á)-(4.09%), 9,19-cyclochloes- tene- 3, 7-diol,4, 14-dimethyl-, 3-acetate (4.09%), 9,19-cyclo-25,26-epoxyergostan-3-ol, 4,4,14-trime- thyl-, acetate (4.09%), 3a,6,6,12a-tetramethyl-1-(1-M ethyl-4-(2-methyl-2-oxiran Yl) pentyl)tetradecahy- drO-1 h-cyclopenta (A) cyclopr opa (E) phenanthen-7-Yl acetate (4.0%), 24-norursa-3,12-dien-11-one (3.65%), 4,8,13-cyclotetradecatrien E-1,3-diol,1,5,9-trimethyl- 12-(1-methyl- ethyl) (3.65%), 9,19-cycloergost-24(28)-en- 3-ol, 4,14-dimethyl-, acetate (3á,4à,5à)-(3.65%), tetrahy- drodammaradienol (3.16%), and acetyl betulinaldehyde (3.16%).

Table (1): The mode of action for identified compounds by GC-MS secreted by *Streptococcus equinus*WC_1.

RT	Area %	Component	Mode of action	Chemical class	Molecular Formula
23.47	1.28	Dasycarpidan-1-Methanol, Acetate (Ester)	It is included in the synthesis of amino acids and plant hormones. 2- It plays an important **role** in the breathing process.		$C_{20}H_{26}N_2O_2$
32.28	3.53	Lup-20(29)-En-3-Ol, Acetate (3á)-		triterpenes	$C_{32}H_{52}O_2$

32.28	3.53	Lup-20(29)-En-3-Yl Acetate		pentacyclic triterpenes	$C_{32}H_{52}O_2$
33.69	14.49	Lupeol	anticancer, antiprotozoal, anti-inflammatory, antimicrobial and chemopreventive properties [43].	a triterpene	$C_{30}H_{50}O$
29.99	2.52	Methyl Commate D	antimicrobial potential [44].		$C_{32}H_{52}O_2$
26.11	1.85	9-Octadecenoic Acid (Z)-	. It is used commercially in the preparation of oleates and lotions, and as a pharmaceutical solvent. (Stedman, 26th ed)	fatty acid	$C_{18}H_{34}O_2$
26.11	1.85	Oleic Acid	preventing heart disease and reducing cholesterol.	**omega-9 fatty acid**	$C_{18}H_{34}O_2$
26.11	1.85	9-Octadecenoic Acid, 1,2,3-Propanetriyl Ester (E,E,E)-		triglyceride	$C_{33}H_{54}O_3$
26.11	1.85	Cis-13-Eicosenoic Acid	It has a role as a mouse metabolite, a rat metabolite and a plant metabolite.	fatty **acids**	$C_{33}H_{54}O_3$
29.31	5.23	Á-Sitosterol	β-**Sitosterol** is used as a dietary supplement for lowering plasma cholesterol	***lipids***	$C_{29}H_{50}O$
29.31	5.23	Ç-Sitosterol	a sterol methyltransferase inhibitor, an anticholesteremic drug, an antioxidant. Active fraction of Solanum trilobatum; reduces side-effects of radiation-induced toxicity.	phytosterols	$C_{29}H_{50}O$
29.31	5.23	STIGMAST-5-EN-3-OL (3á,24S)-	antioxidants		$C_{29}H_{50}O$

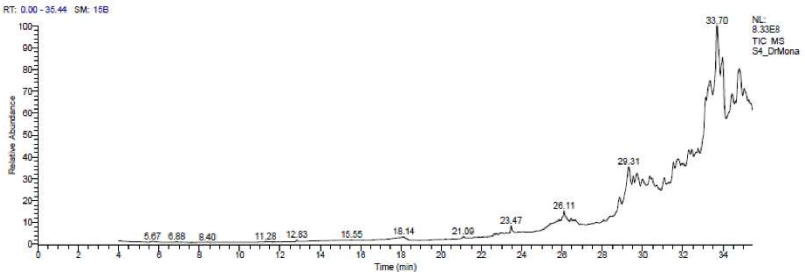


Fig. 1 GC–MS chromatogram of volatile metabolites from *Streptococcus equinus* WC1 (SE-WC1)

Table (2): The mode of action for identified compounds by GC-MS secreted by *Limosilactobacillus reuteri* GM_4.

R.T	Area %.	Component	Mode of action / Biological activity	Chemical class	Chemical formula
23.44	1.77	Hexadecanoic Acid, 2,3-Dihydroxypropyl Ester	**is a natural product found in Isodon eriocalyx, Sigesbeckia glabrescens, and other organisms.**		$C_{19}H_{38}O_4$
23.44	1.77	Hexadecanoic Acid, 2-Hydroxy-1,3-Propanediyl Ester	**is a natural product found** (palmitic) **acid**.		$C_{35}H_{68}O_5$
23.44	1.77	Dasycarpidan-1-Methanol, Acetate (Ester)	2- It plays an important **role** in the breathing process.		C20H26N2O2

28.41	2.89	Lup-20(29)-En-3-Ol, Acetate (3á)-		triterpenes	$C_{32}H_{52}O_2$
28.41	2.89	Lupeol	anticancer, antiprotozoal, anti-inflammatory, antimicrobial and chemopreventive properties [43].	triterpene	$C_{30}H_{50}O$
33.11	5.48	Methyl Commate D	antimicrobial potential [44].		$C_{32}H_{52}O_2$
26.45	1.25	03027205002 Flavone 4'-Oh,5-Oh,7-Di-O-Glucoside		**Flavonoid**	$C_{27}H_{30}O_{15}$
33.11	5.48	1-Heptatriacotanol	antioxidant, anticancer, anti-inflammatory and antimicrobial activity.	alcoholic compound	$C_{37}H_{76}O$
26.45	1.25	7,8-Epoxylanostan-11-Ol, 3-Acetoxy	antioxidant activity; bioactive metabolites.		$C_{32}H_{54}O_4$
26.54	2.97	Fenretinide	inhibits the growth of several human cancer cell lines, acting though both retinoid-receptor-dependent and retinoid-receptor-independent mechanisms. 1In vivo, fenretinide selectively accumulates in breast tissue and is particularly active in inhibiting rat mammary carcinogenesis.		$C_{26}H_{33}NO_2$
26.54	2.97	-15(4-Hydroxyanilino) Retin Al #	vitamers of vitamin A or are chemically related to it. Retinoids have found use in medicine where they regulate epithelial cell growth.	retinoids	$C_{26}H_{33}NO_2$
30.41	3.65	24-Norursa-3,12-Dien-11-One		**Triterpenoids**	$C_{29}H_{44}O$
30.69	1.96	25-Hydroxycholesterol	**.** It has a role as a human metabolite. It derives from a cholesterol**.**	**oxysterol**	$C_{27}H_{46}O_2$
32.88	3.16	Tetrahydrodammaradienol		triterpenoid.	$C_{30}H_{54}O$
32.88	3.16	Acetyl Betulinaldehyde	derivative of the cholesterol biosynthesis inhibitor betulin	a triterpene	$C_{32}H_{50}O_3$
33.11	5.48	Methyl Commate C	anti-inflammatory antimicrobial potential [44].	triterpene	$C_{31}H_{50}O_4$

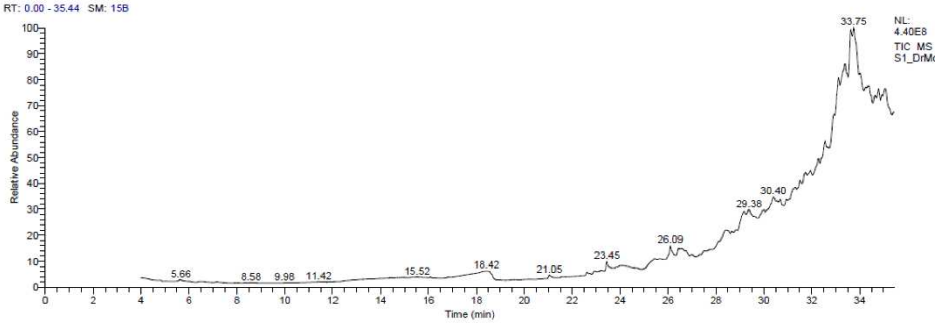


Fig. 2 GC–MS total ion chromatogram (TIC) of volatile metabolites *from Limosilactobacillus reuteri* GM4 (LR-GM4)

2. Molecular docking: *In Silico* Analysis of the Anticancer Potential of Secondary Metabolites from probiotic strains

To characterize the potential protein-binding profiles of the two investigated compounds, SwissTargetPrediction was initially used to identify biologically relevant human protein targets. The most relevant candidates were subsequently examined through structure-based molecular docking. Integrating ligand-based target prediction with receptor-based modelling resulted in the selection of ten functionally diverse proteins for further analysis: the androgen receptor (AR); the dual-specificity phosphatases CDC25A and CDC25B; the G protein-coupled bile acid receptor 1 (GPBAR1); 11β-hydroxysteroid dehydrogenase type 1 (HSD11B1); the constitutive androstane receptor (NR1I3); DNA polymerase beta (POLB); the Hedgehog signaling protein SHH; the cold-sensitive transient receptor potential channel TRPM8; and the phase II drug-metabolizing enzyme UGT2B7. These targets represent several biological categories, including nuclear receptors, regulators of cell-cycle progression, metabolic enzymes, ion channels, and signaling proteins.

The molecular docking results revealed a generally consistent difference in the predicted binding affinities of the two compounds across the investigated targets, as presented in (**Table 3)**. Lupeol showed more favorable binding scores than 1-heptatriacontanol for eight of the ten proteins. Its predicted binding energies ranged from −6.2 kcal/mol for NR1I3 to −11.0 kcal/mol for HSD11B1. In comparison, the docking scores of 1-heptatriacontanol ranged from −3.2 kcal/mol for SHH to −6.8 kcal/mol for UGT2B7. The difference in binding energy between the two compounds, expressed as ΔΔG, varied considerably among the selected targets. The smallest advantage for lupeol was observed with GPBAR1, where the difference was −0.4 kcal/mol, whereas the largest difference was recorded for HSD11B1 at −4.7 kcal/mol. Pronounced differences were also found for AR, SHH, CDC25B, and TRPM8, with ΔΔG values of −4.0, −3.9, −3.4, and −3.0 kcal/mol, respectively.

Table 3. Molecular Docking Binding Affinities (ΔG, kcal/mol)

Target	UniProt ID	1-Heptatriacontanol	Lupeol	ΔΔG (kcal/mol)
AR	P10275	−5.1	−9.1	−4.0
CDC25A	P30304	−4.2	−7.3	−3.1
CDC25B	P30305	−4.3	−7.7	−3.4
GPBAR1	Q8TDU6	−6.3	−6.7	−0.4
HSD11B1	P28845	−6.3	−11.0	−4.7
NR1I3	Q14994	−3.7	−6.2	−2.5
POLB	P06746	−4.5	−7.0	−2.5
SHH	Q15465	−3.2	−7.1	−3.9
TRPM8	Q7Z2W7	−5.4	−8.4	−3.0
UGT2B7	P16662	−6.8	−6.3	+0.5

Among all compound–target combinations, the most favorable docking score was obtained for lupeol against HSD11B1, reaching −11.0 kcal/mol.

Analysis of the docked complex indicated that lupeol was mainly stabilized within the HSD11B1-binding pocket through hydrophobic interactions, as summarized in **(Table 4**). These contacts included alkyl interactions with Val231, Leu217, and Met233, together with a π–alkyl interaction involving Tyr177, as illustrated in **(Fig. 3**).

Table 4. Key Molecular Interactions of Lupeol with Selected Protein Targets

Target	Residue	Interaction	Distance (Å)	Category	Type
HSD11B1	VAL231	A:VAL231···UNL1	5.12	Hydrophobic	Alkyl
	LEU217	UNL1:C···A:LEU217	4.44	Hydrophobic	Alkyl
	MET233	UNL1:C···A:MET233	4.21	Hydrophobic	Alkyl
	TYR177	A:TYR177···UNL1	4.92	Hydrophobic	π–Alkyl
AR	LEU548	UNL1:C···A:LEU548	4.25	Hydrophobic	Alkyl
	PRO549	UNL1:C···A:PRO549	4.68	Hydrophobic	Alkyl
CDC25B	ARG496	A:ARG496:NH1···UNL1:O	2.80	Hydrogen Bond	Conventional H-bond
	PHE271	A:PHE271···UNL1	5.34	Hydrophobic	π–Alkyl
GPBAR1	VAL9	UNL1:H···A:VAL9:O	2.37	Hydrogen Bond	Conventional H-bond
	LEU257	A:LEU257···UNL1	5.49	Hydrophobic	Alkyl
UGT2B7	PHE119	UNL1:C···A:PHE119	3.87	Hydrophobic	π–Sigma
	ILE153	UNL1:C···A:ILE153	4.09	Hydrophobic	Alkyl
	LEU172	UNL1:C···A:LEU172	4.92	Hydrophobic	Alkyl
	HIS35	A:HIS35···UNL1	4.29	Hydrophobic	π–Alkyl
	HIS35	UNL1:C···A:HIS35	4.34	Hydrophobic	π–Alkyl
	PHE174	A:PHE174···UNL1	4.58	Hydrophobic	π–Alkyl
	PHE174	UNL1:C···A:PHE174	4.66	Hydrophobic	π–Alkyl
NR1I3	LEU87	A:LEU87···UNL1	5.40	Hydrophobic	Alkyl
POLB	PHE25	A:PHE25···UNL1	5.36	Hydrophobic	π–Alkyl

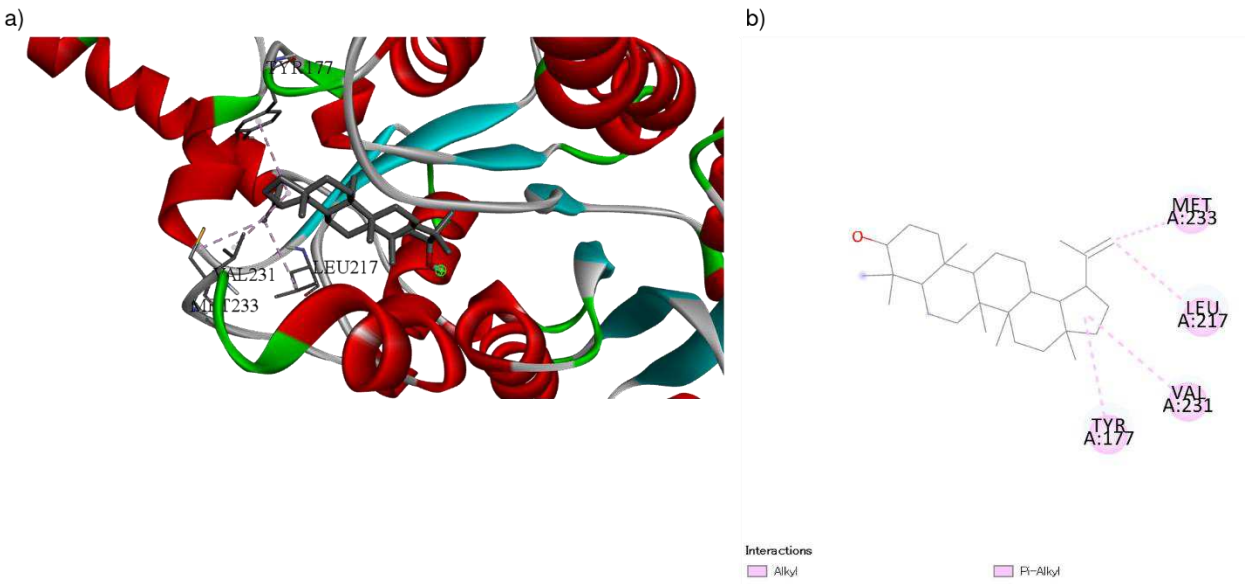


Fig. 3 Molecular docking of lupeol with HSD11B1. (a) Three-dimensional docking pose showing lupeol (grey sticks) bound within the active site of HSD11B1 (ribbon representation: α-helices in red, β-sheets in cyan, loops in green). Key interacting residues are labeled and displayed as sticks: Val231, Leu217, and Met233 form alkyl-type hydrophobic contacts, while Tyr177 engages in a π–alkyl interaction with the ligand. (b) Two-dimensional interaction map depicting the hydrophobic interaction network. Dashed pink lines indicate alkyl interactions with Val231, Leu217, and Met233, and a π–alkyl interaction with Tyr177. The lupeol structure is rendered with its pentacyclic scaffold oriented within the hydrophobic binding cavity

In addition to its strong predicted interaction with HSD11B1, lupeol showed favorable binding patterns with several other proteins included in the receptor panel **(Table 4)**. Within the androgen receptor binding site, lupeol formed hydrophobic alkyl contacts with Leu548 and Pro549 **(Fig. 4)**. As illustrated in the three-dimensional complex **(Fig. 4a)**, the pentacyclic structure of lupeol was accommodated within the hydrophobic ligand-binding pocket, where its orientation allowed close contact with surrounding nonpolar amino acids. The corresponding two-dimensional interaction diagram **(Fig. 4b)** further confirmed these alkyl contacts.

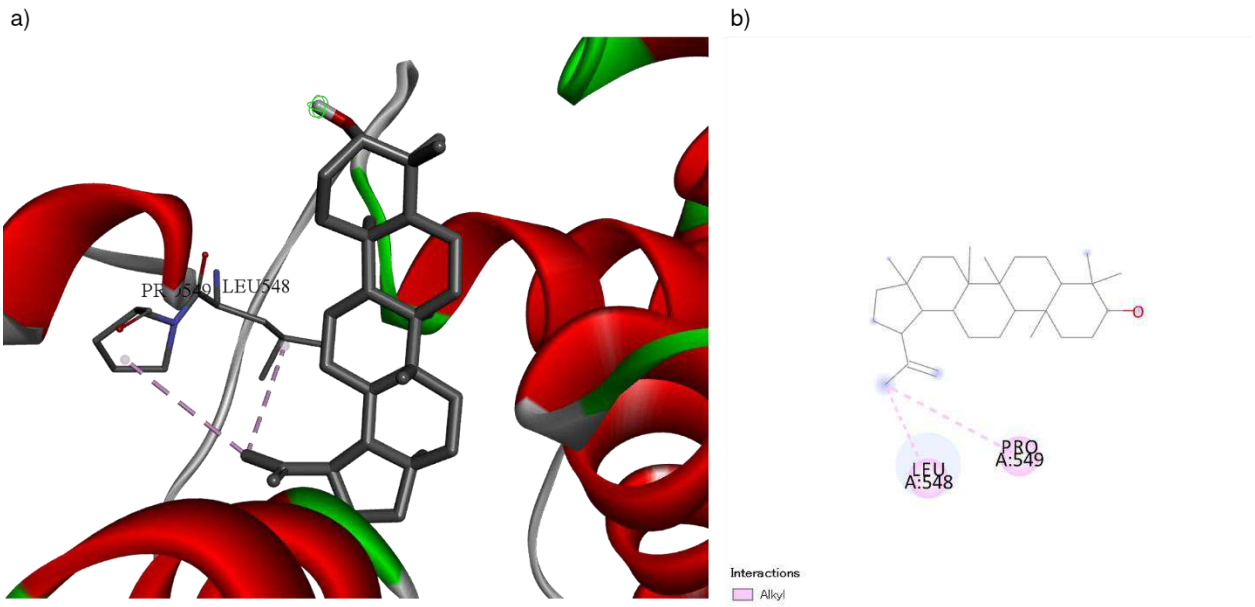


Fig. 4 Molecular docking of lupeol with the androgen receptor (AR). (a) Three-dimensional docking pose showing lupeol (grey sticks) bound within the ligand-binding domain of AR (ribbon representation: α-helices in red, loops in grey). Key interacting residues are labeled and displayed as sticks: Leu548 and Pro549 form alkyl-type hydrophobic contacts with the pentacyclic scaffold of lupeol. (b) Two-dimensional interaction map depicting the hydrophobic interaction network. Dashed pink lines indicate alkyl interactions with Leu548 and Pro549. The lupeol structure is rendered with its rigid pentacyclic core oriented within the hydrophobic binding cavity characteristic of nuclear receptor ligand-binding domains

The cell-cycle regulators CDC25A and CDC25B also showed favorable predicted interactions with lupeol, with docking scores of −7.3 and −7.7 kcal/mol, respectively.

A different interaction pattern was observed for CDC25B. Lupeol formed a conventional hydrogen bond with Arg496 at a distance of 2.80 Å, together with a π–alkyl contact involving Phe271 **(Fig. 5)**. In the three-dimensional docking pose **(Fig. 5a)**, the hydroxyl group of lupeol was oriented toward the guanidinium group of Arg496, enabling hydrogen-bond formation, whereas its pentacyclic framework interacted with the aromatic side chain of Phe271 **(Fig. 5b)**.

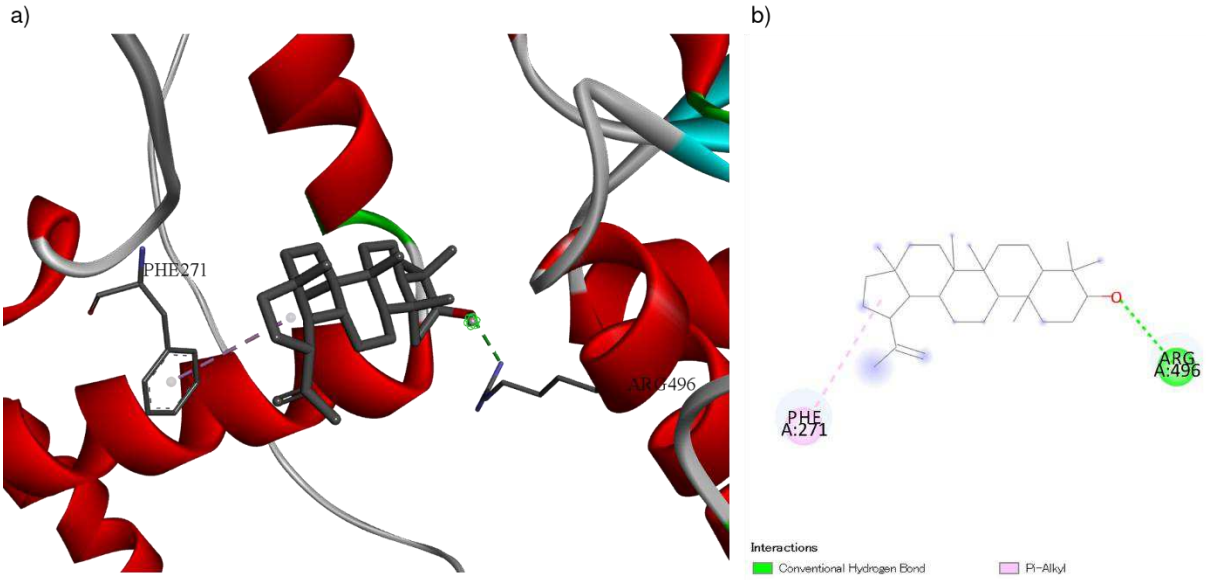


Fig. 5 Molecular docking of lupeol with CDC25B. (a) Three-dimensional docking pose showing lupeol (grey sticks) bound within the catalytic domain of CDC25B (ribbon representation: α-helices in red, loops in grey). Key interacting residues are labeled and displayed as sticks: Arg496 forms a conventional hydrogen bond (green dashed line, 2.80 Å) with the hydroxyl group of lupeol, while Phe271 engages in a π–alkyl interaction with the pentacyclic scaffold. (b) Two-dimensional interaction map depicting the mixed polar-hydrophobic interaction network. The green dashed line indicates the conventional hydrogen bond with Arg496, and the pink dashed line indicates the π–alkyl interaction with Phe271. The lupeol structure is rendered with its hydroxyl group oriented toward the polar residue Arg496 and its hydrophobic core stacked against the aromatic ring of Phe271

For GPBAR1, lupeol displayed a mixed polar and hydrophobic binding pattern. A conventional hydrogen bond was predicted with Val9 at 2.37 Å, while Leu257 contributed an alkyl interaction with the pentacyclic scaffold **(Fig. 6)**. The three-dimensional pose shown in **(Fig. 6a)** placed lupeol near the extracellular region of the receptor. Its hydroxyl group was directed toward the backbone of the N-terminal Val9 residue, whereas the hydrophobic ring system extended further into the transmembrane cavity and contacted Leu257 **(Fig. 6b)**.

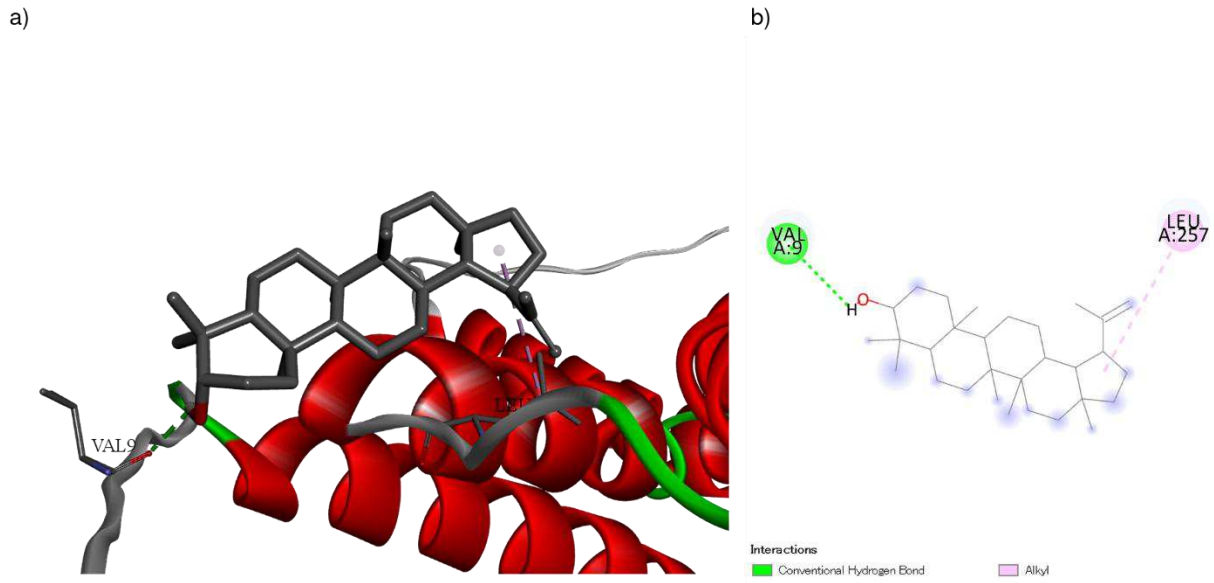


Fig. 6 Molecular docking of lupeol with GPBAR1. (a) Three-dimensional docking pose showing lupeol (grey sticks) bound within the transmembrane domain of GPBAR1 (ribbon representation: α-helices in red, loops in grey). Key interacting residues are labeled and displayed as sticks: Val9 forms a conventional hydrogen bond (green dashed line, 2.37 Å) with the hydroxyl group of lupeol, while Leu257 engages in an alkyl-type hydrophobic interaction with the pentacyclic scaffold. (b) Two-dimensional interaction map depicting the mixed polar-hydrophobic interaction network. The green dashed line indicates the conventional hydrogen bond with Val9, and the pink dashed line indicates the alkyl interaction with Leu257. The lupeol structure is rendered with its hydroxyl group oriented toward the N-terminal Val9 residue and its hydrophobic core extending toward the transmembrane helix containing Leu257

The binding of lupeol to UGT2B7, NR1I3, and POLB was mainly supported by hydrophobic interactions, although the number and distribution of contacts differed considerably among the three targets **(Figs. 7–9)**. In the UGT2B7 complex, lupeol produced a slightly less favorable docking score than 1-heptatriacontanol, yet its binding pose showed a comparatively extensive interaction network. The predicted contacts included π–sigma interactions with Phe119, alkyl interactions with Ile153 and Leu172, and several π–alkyl contacts involving His35 and Phe174 **(Fig. 7)**. As shown in the three-dimensional model **(Fig. 7a)**, lupeol was accommodated within a largely hydrophobic cavity bordered by both aromatic and aliphatic residues. The corresponding two-dimensional diagram **(Fig. 7b)** identified seven individual contacts, representing the most interaction-rich profile observed for lupeol among the evaluated targets.

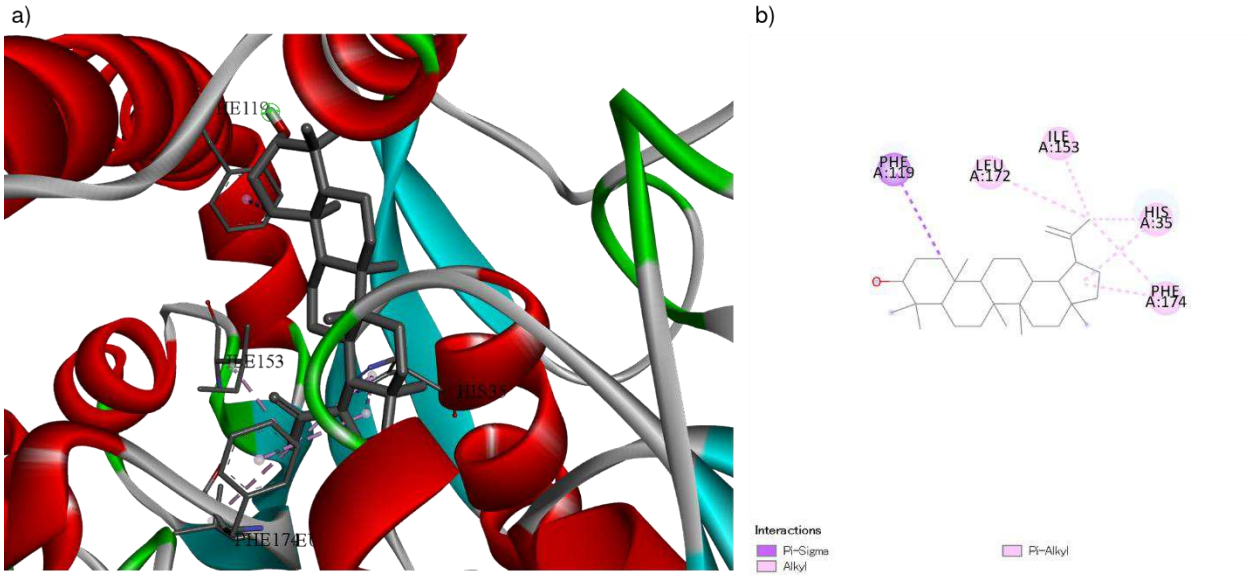


Fig. 7 Molecular docking of lupeol with UGT2B7. (a) Three-dimensional docking pose showing lupeol (grey sticks) bound within the catalytic domain of UGT2B7 (ribbon representation: α-helices in red, β-sheets in cyan, loops in green). Key interacting residues are labeled and displayed as sticks: Phe119 engages in a π–sigma interaction, Ile153 and Leu172 form alkyl-type hydrophobic contacts, and His35 and Phe174 participate in multiple π–alkyl interactions with the pentacyclic scaffold. (b) Two-dimensional interaction map depicting the extensive hydrophobic interaction network. Purple dashed lines indicate π–sigma and π–alkyl interactions with Phe119, His35, and Phe174; pink dashed lines indicate alkyl interactions with Ile153 and Leu172. The lupeol structure is rendered with its pentacyclic core making multiple aromatic and aliphatic contacts within the densely packed active site

A simpler binding pattern was obtained for NR1I3. Lupeol occupied the hydrophobic ligand-binding domain of the nuclear receptor and formed a defined alkyl interaction with Leu87 **(Fig. 8)**. The three-dimensional pose **(Fig. 8a)** placed the pentacyclic scaffold within the nonpolar receptor cavity, whereas the two-dimensional representation **(Fig. 8b)** showed only one prominent directional contact.

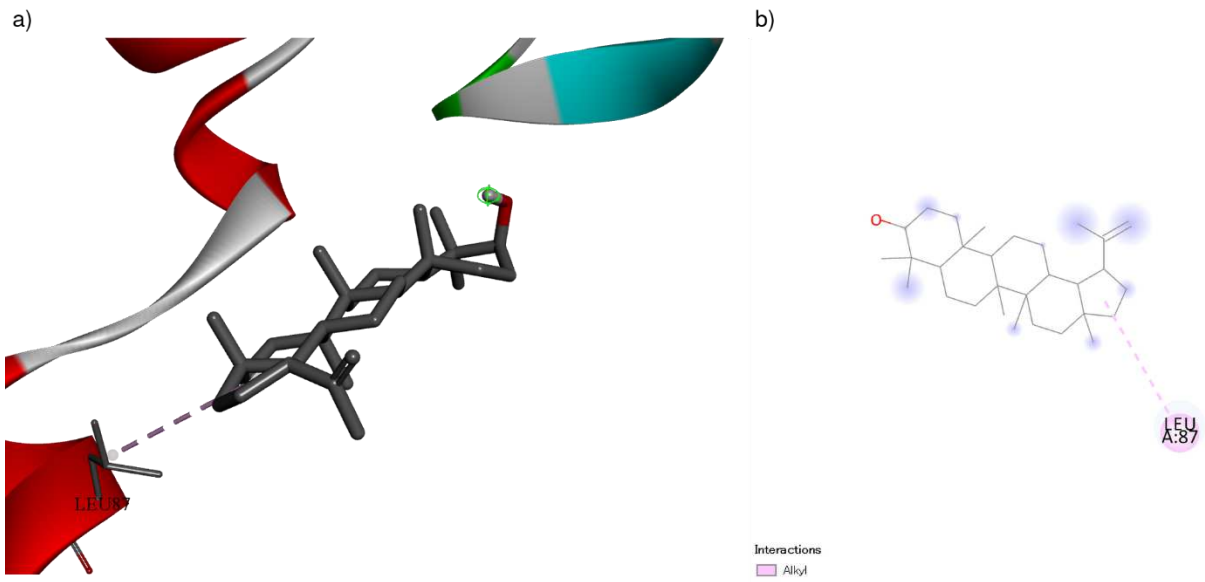


Fig. 8 Molecular docking of lupeol with NR1I3 (constitutive androstane receptor). (a) Three-dimensional docking pose showing lupeol (grey sticks) bound within the ligand-binding domain of NR1I3 (ribbon representation: α-helices in red, β-sheets in cyan, loops in grey). Leu87 forms an alkyl-type hydrophobic contact with the pentacyclic scaffold of lupeol. (b) Two-dimensional interaction map depicting the hydrophobic interaction. The pink dashed line indicates the alkyl interaction with Leu87. The lupeol structure is rendered with its hydrophobic core oriented toward the Leu87 side chain within the ligand-binding pocket

For POLB, lupeol was also stabilized predominantly through nonpolar contacts, with a π–alkyl interaction involving Phe25 forming the principal identified interaction **(Fig. 9)**. In the three-dimensional complex **(Fig. 9a)**, the ligand was positioned close to the region described as the DNA-binding interface, where the pentacyclic scaffold approached the aromatic side chain of Phe25. The two-dimensional map **(Fig. 9b)** additionally indicated van der Waals contacts with Asp91, Ile88, Lys87, Ser94, Lys84, Val29, and Ser30.

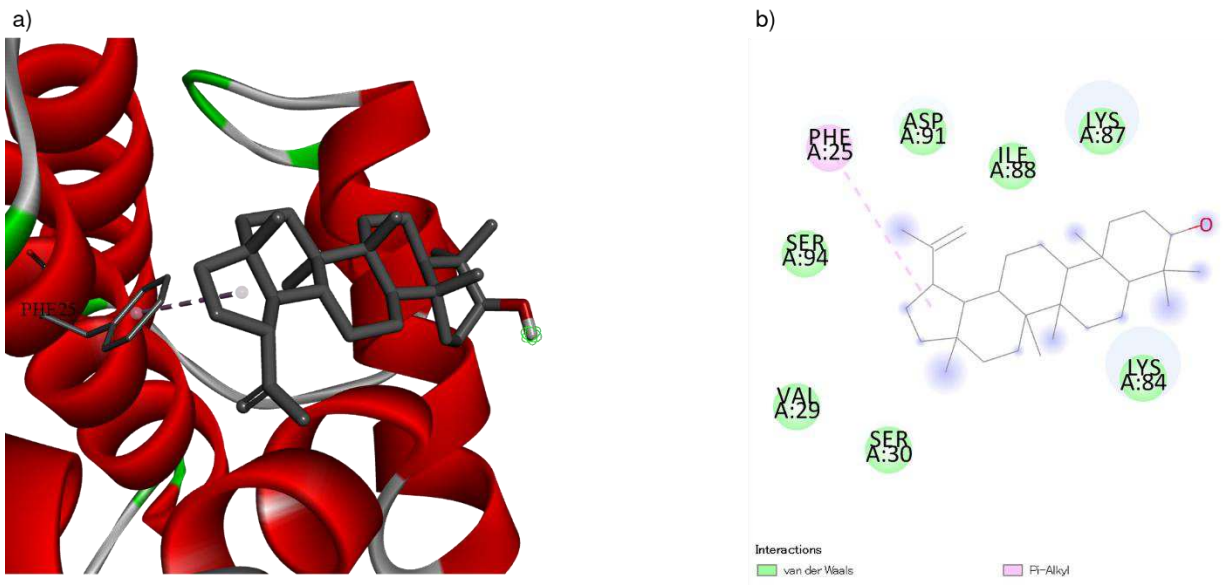


Fig. 9 Molecular docking of lupeol with POLB (DNA polymerase beta). (a) Three-dimensional docking pose showing lupeol (grey sticks) bound within the catalytic domain of POLB (ribbon representation: α-helices in red, loops in grey). Phe25 engages in a π–alkyl interaction with the pentacyclic scaffold of lupeol. Additional surrounding residues (Asp91, Ile88, Lys87, Ser94, Lys84, Val29, Ser30) are shown as green spheres representing van der Waals surface contacts. (b) Two-dimensional interaction map depicting the hydrophobic interaction network. The pink dashed line indicates the π–alkyl interaction with Phe25, while green spheres indicate van der Waals contacts with neighboring residues. The lupeol structure is rendered with its pentacyclic core stacked against the aromatic ring of Phe25 within the DNA-binding/catalytic interface

Lupeol also showed a favorable predicted interaction with TRPM8, with a docking score of −8.4 kcal/mol. The docked complex was supported mainly by van der Waals contacts involving Asp796, Trp798, His845, Gln997, Phe1000, Gln1003, Glu1004, and Ser1007 **(Fig. 10)**. In the three-dimensional model **(Fig. 10A)**, lupeol was accommodated within a largely nonpolar cavity in the transmembrane region of the channel. The two-dimensional interaction map **(Fig. 10B)** did not identify conventional hydrogen bonds or defined π–alkyl contacts, indicating that stabilization of the ligand was primarily associated with multiple nondirectional contacts.

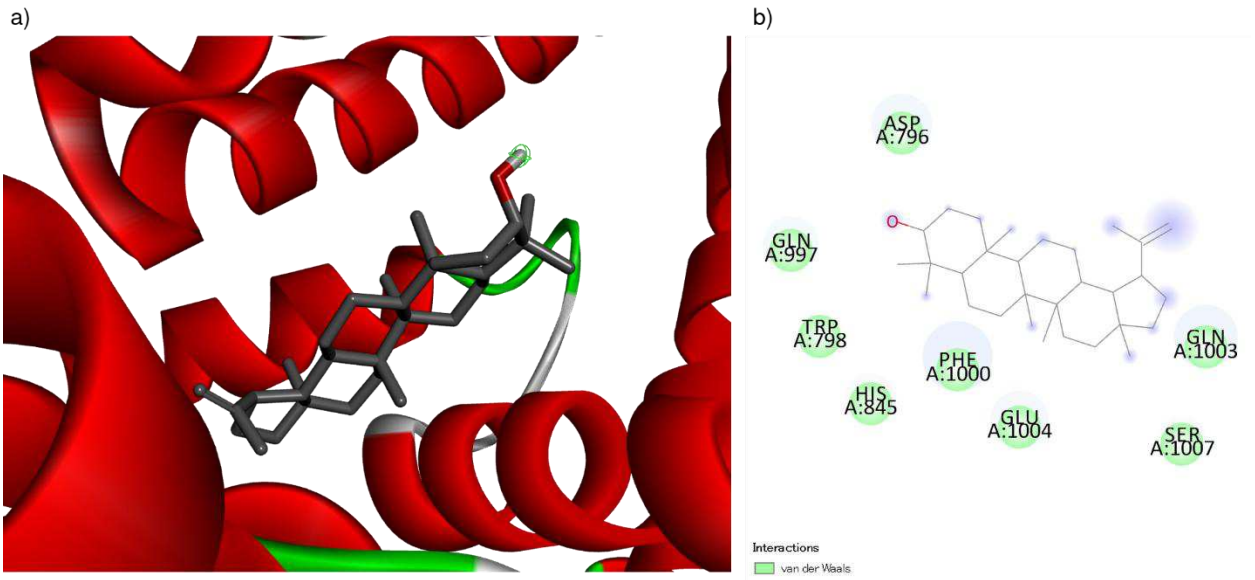


Fig. 10 Molecular docking of lupeol with TRPM8 (transient receptor potential melastatin 8). (a) Three-dimensional docking pose showing lupeol (grey sticks) accommodated within the transmembrane domain of TRPM8 (ribbon representation: α-helices in red, loops in grey). The ligand is positioned within a hydrophobic pocket without forming specific directional interactions. (b) Two-dimensional interaction map depicting van der Waals contacts with surrounding residues. Green spheres indicate non-specific van der Waals interactions with Asp796, Gln997, Trp798, His845, Phe1000, Gln1003, Glu1004, and Ser1007. No hydrogen bonds or π-mediated interactions were detected. The lupeol structure is rendered with its pentacyclic core making non-specific hydrophobic accommodation within the channel pore region

Discussion

1. Anticancer Relevance of Probiotic-Derived Metabolites

Despite the availability of numerous treatments, cancer is still a common illness and the leading cause of death worldwide. The efficacy of cancer treatments has been significantly impacted by the resistance mechanisms that cancer cells have acquired [45–48]. Therefore, newly

active metabolic competent and protein targets should be the focus of new cancer treatments. Lupeol and 1-heptatriacotanol were found to have potential anticancer properties by molecular docking studies.

Lupeol is a triterpene with a number of pharmacological characteristics, including antiprotozoal, anti-inflammatory, anticancer, and antibacterial activity. 1-Heptatriacotanol is an alcoholic molecule with similar characteristics. We can infer that these bacteria may have probiotic potential based on their metabolic activities.

Probiotics may have a part in preventing colon cancer, according to mounting data. Numerous probiotics have been shown in vitro to decrease the proliferation of colon cancer cells. *Lacticaseibacillus paracasei* SP5, *Pediococcus pentosaceus* GS4, and *Pediococcus pentosaceus* SP2. It has been demonstrated that giving mice with colon cancer *Lactobacillus acidophilus* and *Lacticaseibacillus rhamnosus* GG decreases the incidence of tumors. *Lactobacillus acidophilus* and *Lacticaseibacillus rhamnosus* have been shown to improve colon cancer patients' quality of life and reduce gastrointestinal discomfort. Additionally, bacterial fractions and probiotic metabolites may provide protection against colon cancer. It has been shown that *Lacticaseibacillus rhamnosus* cell-free supernatant inhibits HT-29 cell proliferation and metastasis while promoting apoptosis [49, 50].

Probiotic metabolites can arrest the progression of colon cancer. Probiotic supernatants also reduced the activity of matrix metalloproteinase 9 (MMP-9), which is associated with an increased risk of cancer. Supernatants from *Lacticaseibacillus rhamnosus*, *Lactobacillus crispatus*, *Lactobacillus delbrueckii*, and *Limosilactobacillus reuteri* reduced cancer cell invasion by inhibiting cancer cell proliferation, promoting apoptosis, and downregulating MMP-9 expression [51, 52].

Probiotic metabolites, on the other hand, may directly interact with fundamental oncogenic networks to stop growth and trigger apoptosis. *Lactobacillus reuteri* induced tumor-suppressive responses in CT26 cells and the syngeneic (CT26) CRC mice through apoptosis, according to [12]. The treatment concentration and CFU of *Lactobacillus reuteri* were not mentioned by the authors. CT26 vitality was reduced by roughly 50% as a result of both *Lactobacillus reuteri* and cell-free supernatant treatment. The syngeneic (CT26) CRC mouse's tumor weight decreased statistically insignificantly after receiving *Lactobacillus reuteri* (4×10^8 CFU, 3 weeks). Remarkably, the *Lactobacillus reuteri microgel* made with sodium alginate and chitosan demonstrated a tumor weight decrease rate of almost 44%. The control of Bax and Bcl-2 protein expression in CRC mice was demonstrated by Western blot analysis. The pH-resistant probiotic therapy formulation in the treatment of colorectal cancer is highlighted by these molecular findings.

Metabolites generated from probiotics are essential to the therapeutic advantages against colorectal cancer. These microbial chemicals, which include proteins, lipids, carbohydrates, and tiny compounds, directly alter epigenetic pathways, boost antitumor immunity, and reprogram oncogenic signaling to inhibit tumor growth. Metabolites formed from probiotics may encourage

the build-up of reactive oxygen species (ROS) in tumor cells, which may initiate mitochondrial apoptotic pathways.

2. Structural Basis for the Differential Binding of Lupeol and 1-Heptatriacontanol

Such functional diversity is consistent with the poly-pharmacological properties commonly associated with terpenoid compounds derived from plant and microbial sources. Lupeol displayed consistently stronger predicted binding across structurally and functionally diverse proteins, including nuclear receptors, phosphatases, ion channels, and metabolic enzymes. This broad activity suggests that its favorable docking performance may be primarily associated with the physicochemical characteristics of its scaffold rather than with a single target-specific interaction pattern. The rigid pentacyclic framework of lupeol provides a well-defined three-dimensional surface capable of establishing extensive hydrophobic and van der Waals contacts within nonpolar binding pockets. Its amphiphilic character may further support favourable accommodation within chemically heterogeneous active sites. By contrast, 1-heptatriacontanol consists mainly of a long, flexible hydrocarbon chain with limited structural complexity. Although this chain can form hydrophobic contacts, its high conformational flexibility and lack of a compact three-dimensional framework may reduce its ability to achieve stable geometric complementarity within most protein-binding cavities. These structural differences may explain the generally weaker docking scores of 1-heptatriacontanol and the absence of particularly strong predicted interactions across the investigated targets.

3. HSD11B1

This result highlights HSD11B1 as a potentially relevant target for further investigation. HSD11B1 is a microsomal enzyme that catalyses the intracellular conversion of inactive cortisone into active cortisol and therefore plays an important role in the local regulation of glucocorticoid activity. Increased HSD11B1 expression or activity in metabolically active tissues has been linked to visceral adiposity, insulin resistance, and other features of metabolic syndrome, making the enzyme an established target of interest in endocrine and metabolic research. Altered glucocorticoid signaling has also been associated with several aspects of cancer biology, including tumour-cell survival, immune modulation, and resistance to treatment. Accordingly, the predicted interaction between lupeol and HSD11B1 may provide a plausible link between the metabolic and anticancer dimensions of lupeol's polypharmacological profile, although this possibility requires experimental validation in colorectal cancer models.

The interaction with Tyr177 may contribute to the orientation and stabilization of lupeol within the binding cavity. The bulky hydrophobic scaffold of lupeol appears to occupy the pocket through multiple dispersive contacts with surrounding nonpolar residues, while its interaction with the aromatic side chain of Tyr177 may further strengthen ligand accommodation. This binding pattern resembles the predominantly hydrophobic recognition reported for several structurally diverse HSD11B1 ligands identified through virtual-screening and structure-based drug-discovery approaches. Nevertheless, molecular docking does not by itself establish whether lupeol acts through competitive, noncompetitive, or allosteric inhibition. Enzyme-inhibition assays, kinetic

studies, and molecular-dynamics simulations would therefore be needed to confirm the stability and functional consequences of the predicted complex.

4. Androgen Receptor (AR)

This binding pattern is compatible with the general recognition of lipophilic ligands by nuclear receptors, whose binding cavities commonly favor extensive hydrophobic interactions.

5. CDC25A and CDC25B

The simultaneous presence of a polar contact and hydrophobic stabilization may improve ligand retention within the binding pocket. This interaction profile may partly account for the more favorable docking score obtained for lupeol against CDC25B, −7.7 kcal/mol, compared with −4.3 kcal/mol for 1-heptatriacontanol. Although this result suggests possible interference with CDC25B function, confirmation of phosphatase inhibition would require enzyme-based experimental assays.

The geometrically plausible hydrogen-bond distance observed for CDC25B (2.80 Å) suggests that the hydroxyl group of lupeol may act as a polar anchor within the binding region, while the pentacyclic framework contributes additional hydrophobic stabilization through contact with Phe271. This combination of a localized polar interaction and broader hydrophobic accommodation may account for the more favorable docking score of lupeol compared with 1-heptatriacontanol at CDC25B. Because CDC25 phosphatases participate in cyclin-dependent kinase activation and cell-cycle progression, their dysregulation has been associated with uncontrolled proliferation in several cancers, including colorectal malignancies. Consequently, the predicted binding of lupeol to CDC25A and CDC25B provides a plausible basis for investigating whether these phosphatases contribute to its reported antiproliferative activity. Docking alone, however, cannot confirm competitive inhibition, substrate-channel occlusion, G2/M arrest, or apoptosis; these possibilities require direct phosphatase assays and cell-cycle analysis.

6. GPBAR1 (TGR5)

This orientation resembles the general recognition pattern proposed for bile acid-like ligands at GPBAR1, in which a polar functional group interacts near the receptor entrance while the hydrophobic portion of the molecule is accommodated within the transmembrane binding cavity.

GPBAR1, also known as TGR5, participates in bile acid signaling, glucose homeostasis, inflammatory regulation, and energy metabolism, which may lend pharmacological relevance to the predicted interaction with lupeol beyond its structural plausibility. Nevertheless, similarity between the docked orientation of lupeol and those of known GPBAR1 ligands does not establish receptor activation, since docking cannot distinguish an agonist from an antagonist or an inactive binder. Functional assays measuring cyclic AMP production, receptor recruitment, or downstream signaling would therefore be required before assigning lupeol a GPBAR1-modulating role.

7. UGT2B7

Thus, although the docking scores of lupeol and 1-heptatriacontanol were broadly comparable at UGT2B7, lupeol appeared to adopt a more clearly defined orientation involving multiple specific residues. Nevertheless, the greater number of predicted contacts should not be interpreted independently as evidence of stronger biological activity, since docking affinity also depends on ligand conformation, desolvation, and the limitations of the scoring function.

The interaction of lupeol with UGT2B7 also deserves consideration from a pharmacokinetic perspective, since this phase II enzyme mediates glucuronidation reactions relevant to the metabolism and clearance of many xenobiotics and endogenous compounds. A predicted interaction at this site raises the possibility that UGT2B7 could influence the metabolic handling of lupeol itself, a question that would require dedicated metabolic-stability or enzyme-kinetic studies to resolve.

8. NR1I3 (Constitutive Androstane Receptor)

This relatively limited interaction network is consistent with the moderate docking score of −6.2 kcal/mol, which was less favorable than the values obtained for the highest-ranking lupeol targets. The predicted pose therefore suggests that ligand accommodation within NR1I3 may rely largely on nonspecific hydrophobic and van der Waals stabilization rather than on an extensive network of discrete interactions.

NR1I3, the constitutive androstane receptor, regulates the transcription of genes involved in xenobiotic metabolism, including cytochrome P450 enzymes and membrane transporters. The predicted interaction with lupeol therefore suggests a possible, though currently only speculative, connection with pathways governing metabolic detoxification. The relatively simple contact profile and moderate docking score provide limited evidence for a strong interaction, and ligand binding to NR1I3 does not necessarily indicate receptor activation, since transcriptional responses depend on ligand orientation, receptor conformation, co-regulator recruitment, and cellular context.

9. DNA Polymerase Beta (POLB)

Although these contacts lack the directional character of hydrogen bonds, their combined contribution may support the predicted stabilization of lupeol within the binding region. POLB is a central component of the base-excision repair pathway and contributes to the restoration of damaged DNA; its inhibition has therefore been explored as a potential means of increasing the sensitivity of cancer cells to DNA-damaging treatments. The proximity of the docked ligand to residues near the DNA-interacting surface may therefore be of mechanistic interest, but docking alone cannot establish whether lupeol interferes with DNA binding or polymerase activity, and confirmation would require nucleotide-incorporation or DNA-binding assays.

10. TRPM8

Although individually weak, such interactions may collectively support the favorable docking score obtained for this target.

Among these targets, TRPM8 represented an interesting and comparatively unexpected result. This cold-sensitive transient receptor potential channel is activated by low temperature and cooling compounds such as menthol. In addition to its established role in thermal sensation and nociception, altered TRPM8 expression or activity has been reported in several malignancies. The predominantly hydrophobic character of the predicted lupeol–TRPM8 complex is compatible with the lipophilic nature of many known TRPM8 ligands, which occupy nonpolar regions within the transmembrane domain. The favorable docking score therefore raises the possibility that lupeol may interact with TRPM8. However, the present analysis cannot determine whether such an interaction would activate, inhibit, or otherwise alter channel function.

The predicted association with TRPM8 may also be relevant to the reported analgesic and antinociceptive effects of some lupeol-containing natural preparations. Nevertheless, this relationship should presently be regarded as a testable hypothesis rather than an established explanation. Electrophysiological measurements, calcium-flux assays, and experiments using selective TRPM8 antagonists would be necessary to determine whether lupeol directly modulates this channel and whether such modulation contributes to pain-related or anticancer effects.

11. Cross-Target Synthesis

This interaction pattern is consistent with the physicochemical properties of lupeol. Its rigid pentacyclic core is predominantly hydrophobic and provides a broad surface for van der Waals and alkyl-type contacts within nonpolar protein cavities. Polar interactions were less frequent across the investigated targets and were mainly associated with the single hydroxyl group of lupeol. Depending on its orientation and the chemical environment of the binding site, this group may participate as a hydrogen-bond donor or acceptor, as observed in the predicted complexes with CDC25B and GPBAR1. The combination of extensive hydrophobic accommodation and occasional polar anchoring may account for the ability of lupeol to adopt plausible binding poses within several structurally unrelated proteins.

The diversity of the selected targets, including nuclear receptors, cell-cycle regulatory phosphatases, metabolic enzymes, a transient receptor potential channel, and signaling proteins, supports a putative multi-target pharmacological profile. Such behavior has frequently been proposed for structurally complex natural products, particularly terpenoids derived from plants and microorganisms. In relation to colorectal cancer, the predicted target panel may connect lupeol with several biologically relevant processes, including androgen-receptor signaling, cell-cycle progression, glucocorticoid metabolism, xenobiotic processing, DNA repair, and ion-channel regulation. These findings provide a mechanistic framework for considering the potential anticancer relevance of lupeol, but they do not demonstrate that all of the identified proteins are functionally modulated under cellular conditions.

12. Overall Interpretation and Study Limitations

Taken together, the results provide a target-resolved computational overview of the possible pharmacological behavior of lupeol. Rather than identifying a single dominant mechanism, the docking profile suggests that lupeol may interact with several proteins involved in cancer-related signaling, metabolism, cell-cycle regulation, DNA repair, and sensory ion-channel function. The

particularly favorable score at HSD11B1 supports further investigation of glucocorticoid metabolism, whereas the AR and CDC25 results identify potential links with proliferative signaling and cell-cycle control. The GPBAR1, UGT2B7, and NR1I3 complexes point toward possible metabolic and pharmacokinetic effects, while the TRPM8 finding introduces a less explored connection with ion-channel regulation and nociception.

These predictions help organize previously reported biological activities of lupeol within a coherent, testable polypharmacological framework. They should not, however, be viewed as definitive molecular explanations for its metabolic, anti-inflammatory, analgesic, or anticancer effects. Confirmation will require molecular-dynamics simulations, binding and enzyme-inhibition assays, receptor-specific functional studies, cellular uptake measurements, gene- or protein-level validation, and in vivo efficacy models. Such experiments will be essential for determining which of the predicted interactions occur under biological conditions and whether they contribute meaningfully to the anticancer potential of lupeol.

Conclusion

This study integrated ligand-based target prediction with structure-based molecular docking to examine the possible binding profiles of two probiotic-derived metabolites, lupeol and 1-heptatriacontanol, against ten human proteins involved in pathways relevant to colorectal cancer biology. The findings provide a preliminary molecular framework for understanding the potential multi-target behavior of these compounds and for identifying protein targets that merit further experimental investigation.

Across most of the investigated proteins, lupeol produced more favorable docking scores than 1-heptatriacontanol. It showed stronger predicted binding at eight of the ten targets, with differences between the two compounds reaching 4.7 kcal/mol. This overall trend may be related to the compact and rigid pentacyclic scaffold of lupeol, which allows more effective accommodation within hydrophobic protein cavities and supports multiple van der Waals, alkyl, and π-mediated contacts. By comparison, the long and highly flexible carbon chain of 1-heptatriacontanol appears less suited to forming stable and geometrically well-defined interactions within structurally constrained binding pockets.

Among the examined targets, HSD11B1 showed the most favorable predicted interaction with lupeol, with a docking score of −11.0 kcal/mol. The docked complex was mainly stabilized through extensive hydrophobic contacts, including interaction with Tyr177 and several surrounding nonpolar residues. These findings identify HSD11B1 as a particularly interesting candidate for subsequent investigation, especially because local glucocorticoid metabolism has been associated with metabolic dysregulation, tumor-cell adaptation, and treatment response. Nevertheless, the docking results do not establish whether lupeol inhibits HSD11B1 or whether the predicted interaction alters enzyme activity. Enzyme kinetics and target-specific functional assays will therefore be required to determine the biological significance of this binding mode.

The results also suggest that lupeol may exhibit a broad polypharmacological profile involving nuclear receptors, cell-cycle phosphatases, metabolic enzymes, DNA-repair proteins, and ion channels. Such a pattern is consistent with the behavior frequently reported for structurally complex terpenoids, which may interact with several protein families rather than acting through a single molecular target. In colorectal cancer, this type of multi-target activity could be relevant because tumor progression is governed by interconnected processes involving proliferation, metabolism, DNA repair, cellular signaling, and drug response. At present, however, these associations remain predictive and should be regarded as hypotheses for experimental testing.

UGT2B7 represented the only target for which 1-heptatriacontanol showed a marginally more favorable docking score than lupeol. The difference was small, whereas lupeol displayed a denser and more structurally defined interaction network within the predicted binding cavity. This observation illustrates the limitations of relying solely on numerical docking scores. The number, type, orientation, and location of ligand–residue contacts can provide important structural information that may not be reflected fully by a single affinity value. Accordingly, docking scores should be interpreted together with binding poses and residue-level interaction patterns.

Overall, the present findings identify lupeol as the more promising of the two metabolites for further investigation and suggest that probiotic strains capable of producing this compound, including *Limosilactobacillus reuteri* GM4, may represent a source of biologically relevant microbial metabolites. The predicted interactions provide an initial basis for considering lupeol as a potential anti-colorectal cancer candidate with multi-target properties. However, the conclusions of this study remain entirely computational. Validation through molecular-dynamics simulations, direct binding and enzyme-inhibition assays, colorectal cancer cell-based experiments, and in vivo pharmacokinetic and efficacy studies will be necessary to confirm the proposed targets and determine whether lupeol can progress from an in silico candidate to a biologically validated lead compound.

References

1. Weston A, Harris CC (2003) Assessment of Causation by the Bradford-Hill Criteria. In: Kufe D, Pollock R, and Weichselbaum R, et al., editors. Holland- Frei Cancer Medicine. 6th edition. Hamilton (ON): BC Decker; 2003. Available from**:** https://www.ncbi.nlm.nih.gov/books/ NBK13302/

2. Rawla P, Sunkara T, Barsouk A (2019) Epidemiology of colorectal cancer: incidence, mortality, survival, and risk factors. Prz Gastroenterol 14:89–103. https://doi.org/10.5114/pg.2018.81072

3. Dekker E, Tanis PJ, Vleugels JLA, et al (2019) Colorectal cancer. Lancet 394:1467–1480. https://doi.org/10.1016/S0140-6736(19)32319-0

4. Sung H, Ferlay J, Siegel RL, et al (2021) Global Cancer Statistics 2020: GLOBOCAN Estimates of Incidence and Mortality Worldwide for 36 Cancers in 185 Countries. CA Cancer J Clin 71:209–249. https://doi.org/10.3322/caac.21660

5. Kuipers EJ, Grady WM, Lieberman D, et al (2015) Colorectal cancer. Nat Rev Dis Prim 1:1–25. https://doi.org/10.1038/nrdp.2015.65

6. Kim JH (2015) Chemotherapy for colorectal cancer in the elderly. World J Gastroenterol 21:5158–5166. https://doi.org/10.3748/wjg.v21.i17.5158

7. Douaiher J, Ravipati A, Grams B, et al (2017) Colorectal cancer—global burden, trends, and geographical variations. J Surg Oncol 115:619–630. https://doi.org/https://doi.org/10.1002/jso.24578

8. Núñez F P, Quera P R, Gomollón F (2019) Primary sclerosing cholangitis and inflammatory bowel disease: Intestine-liver interrelation. Gastroenterol Hepatol 42:316–325. https://doi.org/10.1016/j.gastrohep.2019.02.004

9. Hamedo HA, Elkashef AA, Mansour MAI, Elshafey N (2023) In vitro and molecular docking studies on a novel Brevibacillus borstelensis NOB3 bioactive compounds as anticancer, anti-inflammatory, and antimicrobial activity. Egypt J Basic Appl Sci 10:518–536. https://doi.org/10.1080/2314808X.2023.2236378

10. Abdelghani Z, Hourani N, Zaidan Z, et al (2021) Therapeutic applications and biological activities of bacterial bioactive extracts. Arch Microbiol 203:4755–4776. https://doi.org/10.1007/s00203-021-02505-1

11. Gibson G, Scott K, Rastall R, et al (2011) Dietary prebiotics: current status and new definition. Food Sci Technol Bull 7:1–19. https://doi.org/10.1616/1476-2137.15880

12. Li N, Niu L, Liu Y, et al (2024) Taking SCFAs produced by Lactobacillus reuteri orally reshapes gut microbiota and elicits antitumor responses. J Nanobiotechnology 22:1–17. https://doi.org/10.1186/s12951-024-02506-4

13. Amin M, Navidifar T, Saeb S, et al (2023) Tumor-targeted induction of intrinsic apoptosis in colon cancer cells by Lactobacillus plantarum and Lactobacillus rhamnosus strains. Mol Biol Rep 50:5345–5354. https://doi.org/10.1007/s11033-023-08445-x

14. Huang L, Zhao Z, Duan C, et al (2019) Lactobacillus plantarum C88 protects against aflatoxin B1-induced liver injury in mice via inhibition of NF-κB-mediated inflammatory responses and excessive apoptosis. BMC Microbiol 19:1–9. https://doi.org/10.1186/s12866-019-1525-4

15. An JJ, Seok H, Ha EM (2021) GABA-producing Lactobacillus plantarum inhibits metastatic properties and induces apoptosis of 5-FU-resistant colorectal cancer cells via GABAB receptor signaling. J Microbiol 59:202–216. https://doi.org/10.1007/s12275-021-0562-5

16. Levy DS, Kahana JA, Kumar R (2009) AKT inhibitor, GSK690693, induces growth inhibition and apoptosis in acute lymphoblastic leukemia cell lines. Blood 113:1723–1729. https://doi.org/10.1182/blood-2008-02-137737

17. Lin L, Ding D, Jiang Y, et al (2018) MEK inhibitors induce apoptosis via FoxO3a-dependent PUMA induction in colorectal cancer cells. Oncogenesis 7:. https://doi.org/10.1038/s41389-018-0078-y

18. Preuss E, Hugle M, Reimann R, et al (2013) Pan-mammalian target of rapamycin (mTOR) inhibitor AZD8055 primes rhabdomyosarcoma cells for ABT-737-induced apoptosis by down-regulating Mcl-1 protein. J Biol Chem 288:35287–35296. https://doi.org/10.1074/jbc.M113.495986

19. Wang X, Martindale JL, Holbrook NJ (2000) Requirement for ERK activation in cisplatin-induced apoptosis. J Biol Chem 275:39435–39443. https://doi.org/10.1074/jbc.M004583200

20. Will M, Qin ACR, Toy W, et al (2014) Rapid induction of apoptosis by PI3K inhibitors is dependent upon their transient inhibition of RAS-ERK signaling. Cancer Discov 4:334–347. https://doi.org/10.1158/2159-8290.CD-13-0611

21. Cocco E, Scaltriti M, Drilon A (2018) NTRK fusion-positive cancers and TRK inhibitor therapy. Nat Rev Clin Oncol 15:731–747. https://doi.org/10.1038/s41571-018-0113-0

22. Fink MY, Chipuk JE (2013) Survival of HER2-Positive Breast Cancer Cells: Receptor Signaling to Apoptotic Control Centers. Genes and Cancer 4:187–195. https://doi.org/10.1177/1947601913488598

23. Goel S, Hidalgo M, Perez-Soler R (2007) EGFR inhibitor-mediated apoptosis in solid tumors. J Exp Ther Oncol 6:305–320

24. Henson ES, Hu X, Gibson SB (2006) Herceptin sensitizes ErbB2-overexpressing cells to apoptosis by reducing antiapoptotic Mcl-1 expression. Clin Cancer Res 12:845–853. https://doi.org/10.1158/1078-0432.CCR-05-0754

25. Jung HY, Joo HJ, Park JK, Kim YH (2012) The Blocking of c-Met signaling induces apoptosis through the increase of p53 protein in lung cancer. Cancer Res Treat 44:251–261. https://doi.org/10.4143/crt.2012.44.4.251

26. Smith KM, Fagan PC, Pomari E, et al (2018) Antitumor Activity of Entrectinib, a Pan-TRK, ROS1, and ALK Inhibitor, in ETV6-NTRK3-Positive Acute Myeloid Leukemia. Mol Cancer Ther 17:455–463. https://doi.org/10.1158/1535-7163.MCT-17-0419

27. Islam MR, Akash S, Rahman MM, et al (2022) Colon cancer and colorectal cancer: Prevention and treatment by potential natural products. Chem Biol Interact 368:110170. https://doi.org/10.1016/j.cbi.2022.110170

28. Eslami M, Yousefi B, Kokhaei P, et al (2019) Importance of probiotics in the prevention and treatment of colorectal cancer. J Cell Physiol 234:17127–17143. https://doi.org/https://doi.org/10.1002/jcp.28473

29. Tong X, Tang R, Xiao M, et al (2022) Targeting cell death pathways for cancer therapy: recent developments in necroptosis, pyroptosis, ferroptosis, and cuproptosis research. J Hematol Oncol 15:174. https://doi.org/10.1186/s13045-022-01392-3

30. Kerry RG, Patra JK, Gouda S, et al (2018) Benefaction of probiotics for human health: A review. J food drug Anal 26:927–939. https://doi.org/10.1016/j.jfda.2018.01.002

31. Kahouli I, Tomaro-Duchesneau C, Prakash S (2013) Probiotics in colorectal cancer (CRC) with emphasis on mechanisms of action and current perspectives. J Med Microbiol

62:1107–1123. https://doi.org/10.1099/jmm.0.048975-0

32. Shokryazdan P, Sieo CC, Kalavathy R, et al (2014) Probiotic potential of Lactobacillus strains with antimicrobial activity against some human pathogenic strains. Biomed Res Int 2014:927268. https://doi.org/10.1155/2014/927268

33. Pinzi L, Rastelli G (2019) Molecular Docking: Shifting Paradigms in Drug Discovery. Int J Mol Sci 20:. https://doi.org/10.3390/ijms20184331

34. Azizoglu U, Argentel-Martínez L, Peñuelas-Rubio O, et al (2025) Natural Products Produced by the Species of Bacillus cereus Group: Recent Updates. J Basic Microbiol 65:e2400666. https://doi.org/https://doi.org/10.1002/jobm.202400666

35. Abdel-Wahhab MA, El-Nekeety AA, Hathout AS, et al (2020) Secondary metabolites from Bacillus sp. MERNA97 extract attenuates the oxidative stress, genotoxicity and cytotoxicity of aflatoxin B1 in rats. Food Chem Toxicol 141:111399. https://doi.org/10.1016/j.fct.2020.111399

36. El-Nekeety AA, Salman AS, Hathout AS, et al (2017) Evaluation of the bioactive extract of actinomyces isolated from the Egyptian environment against aflatoxin B1-induce cytotoxicity, genotoxicity and oxidative stress in the liver of rats. Food Chem Toxicol 105:241–255. https://doi.org/10.1016/j.fct.2017.04.024

37. Halgren TA (1996) Merck molecular force field. I. Basis, form, scope, parameterization, and performance of MMFF94. J Comput Chem 17:490–519. https://doi.org/https://doi.org/10.1002/(SICI)1096-987X(199604)17:5/6<490::AID-JCC1>3.0.CO;2-P

38. Hanwell MD, Curtis D, Lonie D, et al (2012) Avogadro: an open-source molecular builder and visualization tool. J Cheminfo 4:4:17

39. Daina A, Michielin O, Zoete V (2019) SwissTargetPrediction: updated data and new features for efficient prediction of protein targets of small molecules. Nucleic Acids Res 47:W357–W3664. https://doi.org/10.1093/nar/gkz382

40. Liu Y, Yang X, Gan J, et al (2022) CB-Dock2: improved protein-ligand blind docking by integrating cavity detection, docking and homologous template fitting. Nucleic Acids Res 50:W159–W164. https://doi.org/10.1093/nar/gkac394

41. Morris GM, Huey R, Lindstrom W, et al (2009) AutoDock4 and AutoDockTools4: Automated docking with selective receptor flexibility. J Comput Chem 30:2785–2791. https://doi.org/https://doi.org/10.1002/jcc.21256

42. Alhossary A, Handoko SD, Mu Y, Kwoh CK (2015) Fast, accurate, and reliable molecular docking with QuickVina 2. Bioinformatics 31:2214–2216. https://doi.org/10.1093/bioinformatics/btv082

43. Gallo MBC, Sarachine MJ (2009) Biological activities of lupeol. Int J Biomed Pharm Sci 3:46–66

44. Fatima N, Rizwan M, Hobani YH, et al (2017) Gas chromatography/Mass spectroscopy analysis of Catha edulis Forsk, A psycho stimulant revealed potent solvent dependent

antimicrobial activity. J Pharmacogn Phytochem 6:197–204

45. Haider T, Pandey V, Banjare N, et al (2020) Drug resistance in cancer: mechanisms and tackling strategies. Pharmacol Rep 72:1125–1151. https://doi.org/10.1007/s43440-020-00138-7

46. Mansoori B, Mohammadi A, Davudian S, et al (2017) The Different Mechanisms of Cancer Drug Resistance: A Brief Review. Adv Pharm Bull 7:339–348. https://doi.org/10.15171/apb.2017.041

47. Nikolaou M, Pavlopoulou A, Georgakilas AG, Kyrodimos E (2018) The challenge of drug resistance in cancer treatment: a current overview. Clin Exp Metastasis 35:309–318. https://doi.org/10.1007/s10585-018-9903-0

48. Nussinov R, Tsai C-J, Jang H (2021) Anticancer drug resistance: An update and perspective. Drug Resist Updat Rev Comment Antimicrob Anticancer Chemother 59:100796. https://doi.org/10.1016/j.drup.2021.100796

49. Nouri Z, Karami F, Neyazi N, et al (2016) Dual Anti-Metastatic and Anti-Proliferative Activity Assessment of Two Probiotics on HeLa and HT-29 Cell Lines. Cell J 18:127–134. https://doi.org/10.22074/cellj.2016.4307

50. Sharaf LK, Sharma M, Chandel D, Shukla G (2018) Prophylactic intervention of probiotics (L.acidophilus, L.rhamnosus GG) and celecoxib modulate Bax-mediated apoptosis in 1,2-dimethylhydrazine-induced experimental colon carcinogenesis. BMC Cancer 18:1111. https://doi.org/10.1186/s12885-018-4999-9

51. Wan Y, Xin Y, Zhang C, et al (2014) Fermentation supernatants of Lactobacillus delbrueckii inhibit growth of human colon cancer cells and induce apoptosis through a caspase 3-dependent pathway. Oncol Lett 7:1738–1742. https://doi.org/10.3892/ol.2014.1959

52. Maghsood F, Johari B, Rohani M, et al (2020) Anti-proliferative and Anti-metastatic Potential of High Molecular Weight Secretory Molecules from Probiotic Lactobacillus Reuteri Cell-Free Supernatant Against Human Colon Cancer Stem-Like Cells (HT29-ShE). Int J Pept Res Ther 26:2619–2631. https://doi.org/10.1007/s10989-020-10049-z

Figure captions

-Fig. 1 GC–MS chromatogram of volatile metabolites from *Streptococcus equinus* WC1 (SE-WC1)

- **Fig. 2** GC–MS total ion chromatogram (TIC) of volatile metabolites *from Limosilactobacillus reuteri* GM4 (LR-GM4)

-**Fig.** 3 Molecular docking of lupeol with HSD11B1. (a) Three-dimensional docking pose showing lupeol (grey sticks) bound within the active site of HSD11B1 (ribbon representation: α-helices in red, β-sheets in cyan, loops in green). Key interacting residues are labeled and displayed as sticks: Val231, Leu217, and Met233 form alkyl-type hydrophobic contacts, while Tyr177 engages in a

π–alkyl interaction with the ligand. (b) Two-dimensional interaction map depicting the hydrophobic interaction network. Dashed pink lines indicate alkyl interactions with Val231, Leu217, and Met233, and a π–alkyl interaction with Tyr177. The lupeol structure is rendered with its pentacyclic scaffold oriented within the hydrophobic binding cavity

-**Fig. 4** Molecular docking of lupeol with the androgen receptor (AR). (a) Three-dimensional docking pose showing lupeol (grey sticks) bound within the ligand-binding domain of AR (ribbon representation: α-helices in red, loops in grey). Key interacting residues are labeled and displayed as sticks: Leu548 and Pro549 form alkyl-type hydrophobic contacts with the pentacyclic scaffold of lupeol. (b) Two-dimensional interaction map depicting the hydrophobic interaction network. Dashed pink lines indicate alkyl interactions with Leu548 and Pro549. The lupeol structure is rendered with its rigid pentacyclic core oriented within the hydrophobic binding cavity characteristic of nuclear receptor ligand-binding domains

-**Fig. 5** Molecular docking of lupeol with CDC25B. (a) Three-dimensional docking pose showing lupeol (grey sticks) bound within the catalytic domain of CDC25B (ribbon representation: α-helices in red, loops in grey). Key interacting residues are labeled and displayed as sticks: Arg496 forms a conventional hydrogen bond (green dashed line, 2.80 Å) with the hydroxyl group of lupeol, while Phe271 engages in a π–alkyl interaction with the pentacyclic scaffold. (b) Two-dimensional interaction map depicting the mixed polar-hydrophobic interaction network. The green dashed line indicates the conventional hydrogen bond with Arg496, and the pink dashed line indicates the π–alkyl interaction with Phe271. The lupeol structure is rendered with its hydroxyl group oriented toward the polar residue Arg496 and its hydrophobic core stacked against the aromatic ring of Phe271

-**Fig. 6** Molecular docking of lupeol with GPBAR1. (a) Three-dimensional docking pose showing lupeol (grey sticks) bound within the transmembrane domain of GPBAR1 (ribbon representation: α-helices in red, loops in grey). Key interacting residues are labeled and displayed as sticks: Val9 forms a conventional hydrogen bond (green dashed line, 2.37 Å) with the hydroxyl group of lupeol, while Leu257 engages in an alkyl-type hydrophobic interaction with the pentacyclic scaffold. (b) Two-dimensional interaction map depicting the mixed polar-hydrophobic interaction network. The green dashed line indicates the conventional hydrogen bond with Val9, and the pink dashed line indicates the alkyl interaction with Leu257. The lupeol structure is rendered with its hydroxyl group oriented toward the N-terminal Val9 residue and its hydrophobic core extending toward the transmembrane helix containing Leu257

-**Fig. 7** Molecular docking of lupeol with UGT2B7. (a) Three-dimensional docking pose showing lupeol (grey sticks) bound within the catalytic domain of UGT2B7 (ribbon representation: α-helices in red, β-sheets in cyan, loops in green). Key interacting residues are labeled and displayed as sticks: Phe119 engages in a π–sigma interaction, Ile153 and Leu172 form alkyl-type hydrophobic contacts, and His35 and Phe174 participate in multiple π–alkyl interactions with the pentacyclic scaffold. (b) Two-dimensional interaction map depicting the extensive hydrophobic interaction network. Purple dashed lines indicate π–sigma and π–alkyl interactions with Phe119, His35, and Phe174; pink dashed lines indicate alkyl interactions with Ile153 and Leu172. The

lupeol structure is rendered with its pentacyclic core making multiple aromatic and aliphatic contacts within the densely packed active site

-**Fig. 8** Molecular docking of lupeol with NR1I3 (constitutive androstane receptor). (a) Three-dimensional docking pose showing lupeol (grey sticks) bound within the ligand-binding domain of NR1I3 (ribbon representation: α-helices in red, β-sheets in cyan, loops in grey). Leu87 forms an alkyl-type hydrophobic contact with the pentacyclic scaffold of lupeol. (b) Two-dimensional interaction map depicting the hydrophobic interaction. The pink dashed line indicates the alkyl interaction with Leu87. The lupeol structure is rendered with its hydrophobic core oriented toward the Leu87 side chain within the ligand-binding pocket

-**Fig. 9** Molecular docking of lupeol with POLB (DNA polymerase beta). (a) Three-dimensional docking pose showing lupeol (grey sticks) bound within the catalytic domain of POLB (ribbon representation: α-helices in red, loops in grey). Phe25 engages in a π–alkyl interaction with the pentacyclic scaffold of lupeol. Additional surrounding residues (Asp91, Ile88, Lys87, Ser94, Lys84, Val29, Ser30) are shown as green spheres representing van der Waals surface contacts. (b) Two-dimensional interaction map depicting the hydrophobic interaction network. The pink dashed line indicates the π–alkyl interaction with Phe25, while green spheres indicate van der Waals contacts with neighboring residues. The lupeol structure is rendered with its pentacyclic core stacked against the aromatic ring of Phe25 within the DNA-binding/catalytic interface

-**Fig. 10** Molecular docking of lupeol with TRPM8 (transient receptor potential melastatin 8). (a) Three-dimensional docking pose showing lupeol (grey sticks) accommodated within the transmembrane domain of TRPM8 (ribbon representation: α-helices in red, loops in grey). The ligand is positioned within a hydrophobic pocket without forming specific directional interactions. (b) Two-dimensional interaction map depicting van der Waals contacts with surrounding residues. Green spheres indicate non-specific van der Waals interactions with Asp796, Gln997, Trp798, His845, Phe1000, Gln1003, Glu1004, and Ser1007. No hydrogen bonds or π-mediated interactions were detected. The lupeol structure is rendered with its pentacyclic core making non-specific hydrophobic accommodation within the channel pore region